Journal of Power Sources 196 (2011) 4996–4999

Contents lists available at ScienceDirect

Journal of Power Sources

journal homepage: www.elsevier.com/locate/jpowsour

Short communication

Electrical conductivity of $Ce_{0.8}Gd_{0.2-x}Dy_xO_{2-\delta}$ ($0 \le x \le 0.2$) co-doped with Gd^{3+} and Dy^{3+} for intermediate-temperature solid oxide fuel cells

K. Park*, H.K. Hwang

Faculty of Nanotechnology and Advanced Materials Engineering, Sejong University, Seoul 143-747, Republic of Korea

ARTICLE INFO

Article history:
Received 26 August 2010
Received in revised form 12 January 2011
Accepted 14 January 2011
Available online 16 February 2011

Keywords:
Nano-sized powder
Solution combustion process
Electrical conductivity
Microstructure
Ceria
Intermediate-temperature solid oxide fuel cells

ABSTRACT

High-quality nano-sized $Ce_{0.8}Gd_{0.2-x}Dy_xO_{2-\delta}$ ($0 \le x \le 0.2$) powders are synthesized by a solution combustion process. The calcined powders are composed of a ceria-based single phase with a cubic fluorite structure and are nanocrystalline nature, i.e., 15–24 nm in crystallite size. The addition of an intermediate amount of Dy^{3+} ($0.03 \le x \le 0.16$) for Gd^{3+} in $Ce_{0.8}Gd_{0.2}O_{2-\delta}$ decreases the electrical conductivity. On the other hand, the doping of a small amount of Dy^{3+} ($0.01 \le x \le 0.02$) and of a large amount of Dy^{3+} ($0.17 \le x \le 0.19$) leads to an increase in conductivity. The $Ce_{0.8}Gd_{0.03}Dy_{0.17}O_{2-\delta}$ shows the highest electrical conductivity (0.215 S cm^{-1}) at 800 °C.

1. Introduction

Solid oxide fuel cells (SOFCs) convert chemical energy directly into electrical energy with high efficiency, environmental friendliness, and great flexibility in the choice of fuel. Conventional SOFCs which use yttria stabilized zirconia (YSZ) as an electrolyte material are operated at ~1000 °C. Lowering the operating temperature to an intermediate temperature (500–800 °C) significantly enhances the long-term performance stability, widens the material selection, lessens the sealing problem, and allows the use of low-cost metallic interconnects, thereby accelerating the commercialization of SOFC technology [1]. In this study, a ceria-based oxide is selected as an electrolyte material for intermediate-temperature solid oxide fuel cells (IT-SOFCs).

In addition, a solution combustion process is considered to be effective in synthesizing ceria-based nanopowders. The method involves the dissolution of metal nitrate and combustion fuel in water, and then heating of the resulting solution [2,3]. After the solution reaches the temperature of spontaneous combustion, it begins burning and becomes a powder. This method is particularly useful in the production of ultra-fine ceramic powders of complex oxide compositions in a relatively short time [2,3].

One of the most favourable dopants in ceria-based electrolytes is Gd^{3+} [4,5]. The conductivity of $Ce_{0.8}Gd_{0.2}O_{2-\delta}$ was much greater than that of conventional 8 mol% Y-doped YSZ. In addition, Dy^{3+} was used as a promising dopant in ceria [6]. The conductivity of $Ce_{0.9}Dy_{0.1}O_{2-\delta}$ was slightly lower than that of $Ce_{0.9}Gd_{0.1}O_{2-\delta}$ at 700 °C. The electrical conductivity of $Ce_{1-x}Dy_xO_{2-\delta}$ increases with increase in the Dy^{3+} content and reaches a maximum at $x = 0.3$. Several workers have investigated the effects of co-doping on the electrical properties of ceria-based electrolytes [7,8]. The co-doping technique has been widely accepted as an effective method for improving the conductivity of ceria. The present study examines the effect of Gd^{3+} and Dy^{3+} co-doping on the electrical conductivity of ceria-based electrolytes.

2. Experimental

A series of nano-sized $Ce_{0.8}Gd_{0.2-x}Dy_xO_{2-\delta}$ ($0 \le x \le 0.2$) powders was synthesized by the combustion synthesis process in which $Ce(NO_3)_3 \cdot 6H_2O$, $Gd(NO_3)_3 \cdot 5H_2O$, and $Dy(NO_3)_3 \cdot 5H_2O$ were used as oxidizers and aspartic acid ($C_4H_7NO_4$) as fuel. The metal nitrates were dissolved separately in distilled water to form homogeneous solutions. The aspartic acid was dissolved in the solutions to prepare a transparent aqueous solution. The molar ratio of the metal nitrates to aspartic acid was controlled at 1:1. The resultant solution was slowly heated on a hot plate until a highly viscous gel precursor was obtained. The precursor was heated to 300 °C and then auto-ignited with the rapid evolution of a large volume of gases to

* Corresponding author. Tel.: +82 2 3408 3777; fax: +82 2 3408 4342.
E-mail address: kspark@sejong.ac.kr (K. Park).

0378-7753/$ – see front matter © 2011 Elsevier B.V. All rights reserved.
doi:10.1016/j.jpowsour.2011.01.107

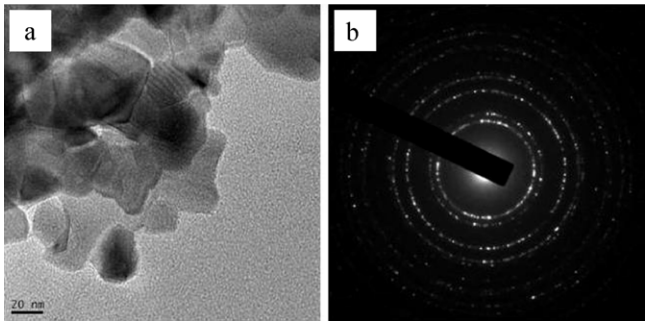

Fig. 1. (a) TEM bright field image and (b) the corresponding SAD pattern of calcined $Ce_{0.8}Gd_{0.2}O_{2-\delta}$ powders.

produce voluminous powders. The obtained powders were ground and then calcined at 300 °C for 4 h. The size and morphology of the synthesized and calcined powders were investigated with a transmission electron microscope (TEM; JEM-2100F, JEOL) that operated at 200 kV.

The calcined powders were cold-pressed under 150 MPa to prepare green pellets. The pellets were heated at 1400 °C for 5 h in air and then furnace cooled. The crystal structure of the calcined powders and sintered pellets were analyzed with an X-ray diffractometer (XRD; Rigaku DMAX 2500) using Cu Kα radiation at 40 kV and 100 mA. The microstructure of the sintered pellets was investigated with a field emission scanning electron microscope (FE-SEM, Hitachi S-4700). The density of the sintered pellets was measured by the Archimedes method. Samples for the measurements of electrical conductivity were cut out of the sintered bodies in the form of rectangular bars with dimensions of 4 mm × 4 mm × 20 mm using a diamond saw, and then polished with SiC emery papers. The electrical conductivity of each sintered body was measured over a temperature range of 400–800 °C in air using the direct current four-probe method (Zahner Messtechnik, IM6e, Germany).

3. Results and discussion

Fig. 1(a) and (b) shows a TEM bright field image and its corresponding selected area diffraction (SAD) pattern for the calcined $Ce_{0.8}Gd_{0.2}O_{2-\delta}$ powders, respectively. The size of the calcined $Ce_{0.8}Gd_{0.2}O_{2-\delta}$ powder measured from the image is in nano-scale, i.e., 22 nm. The average sizes of the other calcined Gd^{3+} and Dy^{3+} co-doped powders are between 15 and 24 nm (not shown here). In general, the powder size significantly affects the sintering behaviour. The driving force for sintering originates from the reduction in the total free energy ΔG_t as follows [9]:

$$\Delta G_t = \Delta G_v + \Delta G_b + \Delta G_s \quad (1)$$

where ΔG_v, ΔG_b, ΔG_s are the changes in free energy associated with the volume, boundary and surface of grains, respectively. The primary driving force in sintering is the ΔG_s, but the other terms may be important for some material systems. The smaller powder has a larger surface energy, thus allowing a larger densification rate and a grain growth rate because of a high diffusivity near the surface and grain boundary during sintering [10]. In changing the powder size from a 10 to 1 μm, the sintering rate was increased by a factor of 10 [11].

The nanostructured features of the calcined powders lower the sintering temperature. Nevertheless, the nano-sized $Ce_{0.8}Gd_{0.2-x}Dy_xO_{2-\delta}$ powders allow a high density and ultra-fine grain size. Conventional large sized powders do not sinter well, even at temperatures as high as 1650 °C [12]. Lowering the sintering temperature of ceria-based electrolytes might enhance the possibility of co-sintering of electrolyte and electrodes. Obviously, this aspartic acid-assisted combustion process is highly effective in synthesizing high-quality $Ce_{0.8}Gd_{0.2-x}Dy_xO_{2-\delta}$ nano-sized powders, compared with the conventional solid-state reaction process.

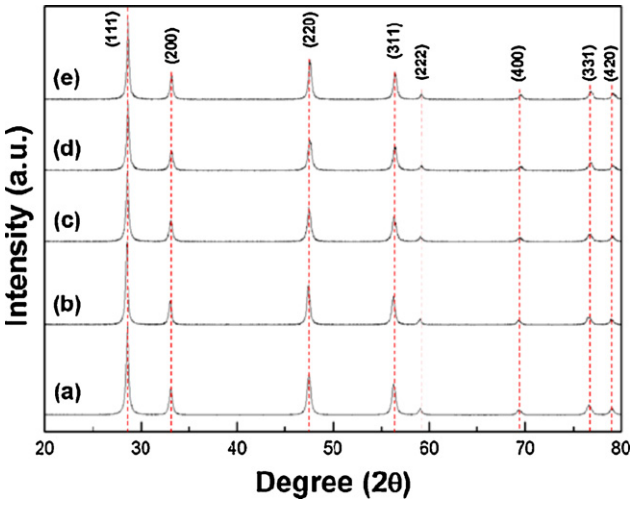

Fig. 2. XRD patterns of calcined $Ce_{0.8}Gd_{0.2-x}Dy_xO_{2-\delta}$ powders with x = (a) 0, (b) 0.05, (c) 0.1, (d) 0.15, and (e) 0.2.

The XRD patterns of calcined $Ce_{0.8}Gd_{0.2-x}Dy_xO_{2-\delta}$ ($0 \le x \le 0.2$) powders are given in Fig. 2. The calcined $Ce_{0.8}Gd_{0.2-x}Dy_xO_{2-\delta}$ powders form a ceria-based single phase with the cubic fluorite structure [13]. No un-reacted oxides are detected. These results indicate that the co-doped Gd^{3+} and Dy^{3+} are present in the ceria crystal lattice to form solid solutions. The calcined powders have the same crystal structure, irrespective of Dy^{3+} content, except for the position of XRD peaks. The substitution of Gd^{3+} by Dy^{3+} causes the diffracted peaks to shift slightly toward higher angles and this indicates a slight decrease in the lattice constant. This is because the radius of Dy^{3+} (0.103 nm) is smaller than that of Gd^{3+} (0.106 nm) [14].

The crystallite size (D) of the calcined powders was calculated from the Scherrer formula [15]: $D = (0.9\lambda)/(\beta \cos\theta)$, where λ is the wavelength of radiation, θ is the angle of the diffraction peak, and β is the full width at half-maximum of the diffraction peak (in radian). The calculated crystallite sizes are in the range of 22.6–24.5 nm, which are similar to those of the calcined $Ce_{0.8}Gd_{0.2}O_{2-\delta}$ powders illustrated in Fig. 1, indicating a nanocrystalline nature. There is no apparent compositional dependence on the powder size.

The XRD peaks are sharpened after sintering at 1400 °C for 5 h in air, as shown in Fig. 3 and this represents an increased crystallite size and improved crystallinity. The crystal structure of the sintered $Ce_{0.8}Gd_{0.2-x}Dy_xO_{2-\delta}$ pellets is basically equivalent to that of the calcined powders of the same compositions discussed previously. As expected, the peaks of the sintered pellets shift slightly towards higher angles when the value of x increased from 0 to 0.2. The lattice constants of the sintered $Ce_{0.8}Gd_{0.2-x}Dy_xO_{2-\delta}$ with x = 0, 0.05, 0.1, 0.15, and 0.2 are 5.417, 5.416, 5.411, 5.404 and 5.402 Å, respectively.

Typical FE-SEM images of the single-doped $Ce_{0.8}Gd_{0.2}O_{2-\delta}$ and $Ce_{0.8}Dy_{0.2}O_{2-\delta}$ sintered at 1400 °C are presented in Fig. 4(a) and (b), respectively. The grain size and density of $Ce_{0.8}Gd_{0.2}O_{2-\delta}$ are smaller than those of $Ce_{0.8}Dy_{0.2}O_{2-\delta}$. The mean grain sizes of the $Ce_{0.8}Gd_{0.2}O_{2-\delta}$ and $Ce_{0.8}Dy_{0.2}O_{2-\delta}$ are 349 and 551 nm, respectively, and the densities of the $Ce_{0.8}Gd_{0.2}O_{2-\delta}$ and $Ce_{0.8}Dy_{0.2}O_{2-\delta}$ are 93.3 and 98.7% of the theoretical value, respectively. In addition, the grain size and density of the co-doped samples exhibit the same trend as the single-doped samples. The mean grain sizes of the $Ce_{0.8}Gd_{0.15}Dy_{0.05}O_{2-\delta}$, $Ce_{0.8}Gd_{0.1}Dy_{0.1}O_{2-\delta}$, and $Ce_{0.8}Gd_{0.05}Dy_{0.15}O_{2-\delta}$ are 456, 516, and 536 nm, respectively, and

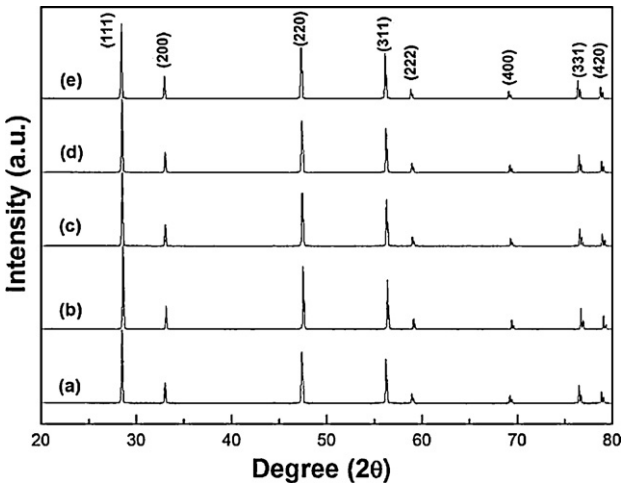

Fig. 3. XRD patterns of sintered $Ce_{0.8}Gd_{0.2-x}Dy_xO_{2-\delta}$ samples with x = (a) 0, (b) 0.05, (c) 0.1, (d) 0.15, and (e) 0.2.

the densities of the $Ce_{0.8}Gd_{0.15}Dy_{0.05}O_{2-\delta}$, $Ce_{0.8}Gd_{0.1}Dy_{0.1}O_{2-\delta}$, and $Ce_{0.8}Gd_{0.05}Dy_{0.15}O_{2-\delta}$ were 95.1, 96.6, and 97.3% of the theoretical density, respectively (not shown here). These results indicate that the grain size and density of the $Ce_{0.8}Gd_{0.2-x}Dy_xO_{2-\delta}$ ($0 \le x \le 0.2$) increase with increase in the Dy^{3+} content. Dy^{3+} substitution enhances the densification rate and the grain growth rate during isothermal sintering at 1400 °C. The substituted Dy^{3+} raises the effective diffusion coefficient, thereby allowing pores to shrink faster and thus to stay attached to grain boundaries during grain growth because smaller pores can migrate faster [16,17]. In addition, an increase in the surface diffusion coefficient accelerates the coarsening.

To optimize the electrical conductivity of ceria-based electrolytes, the electrical conductivity of the Gd^{3+} and Dy^{3+} co-doped $Ce_{0.8}Gd_{0.2-x}Dy_xO_{2-\delta}$ ($0 \le x \le 0.2$) was investigated, as shown in Fig. 5. It is apparent that the $Ce_{0.8}Gd_{0.2-x}Dy_xO_{2-\delta}$ has a much higher conductivity over the measured temperature range, in comparison with YSZ [18]. The electrical conductivity depends strongly on the Dy^{3+} content and temperature. In Fig. 5(a), the electrical conductivity decreases with an increase in Dy^{3+} content, reaching a minimum at x = 0.1, and then increases with a further increase in Dy^{3+} content. This indicates that the conductivity of the co-doped samples is poorer than that of the single-doped sample, i.e., $Ce_{0.8}Gd_{0.2}O_{2-\delta}$ or $Ce_{0.8}Dy_{0.2}O_{2-\delta}$. The electrical conductivities of the $Ce_{0.8}Gd_{0.2-x}Dy_xO_{2-\delta}$ with x = 0, 0.05, 0.1, 0.15, and 0.2 at 800 °C are 0.146, 0.101, 0.090, 0.105, and 0.124 S cm^{-1}, respectively.

When the precise amount of Dy^{3+} for Gd^{3+} in the $Ce_{0.8}Gd_{0.2}O_{2-\delta}$ is doped, a highly enhanced conductivity is obtained, as shown in Fig. 5(b) and (c), which display the electrical conductivities of the $Ce_{0.8}Gd_{0.2-x}Dy_xO_{2-\delta}$ samples with low ($0 \le x \le 0.05$) and high

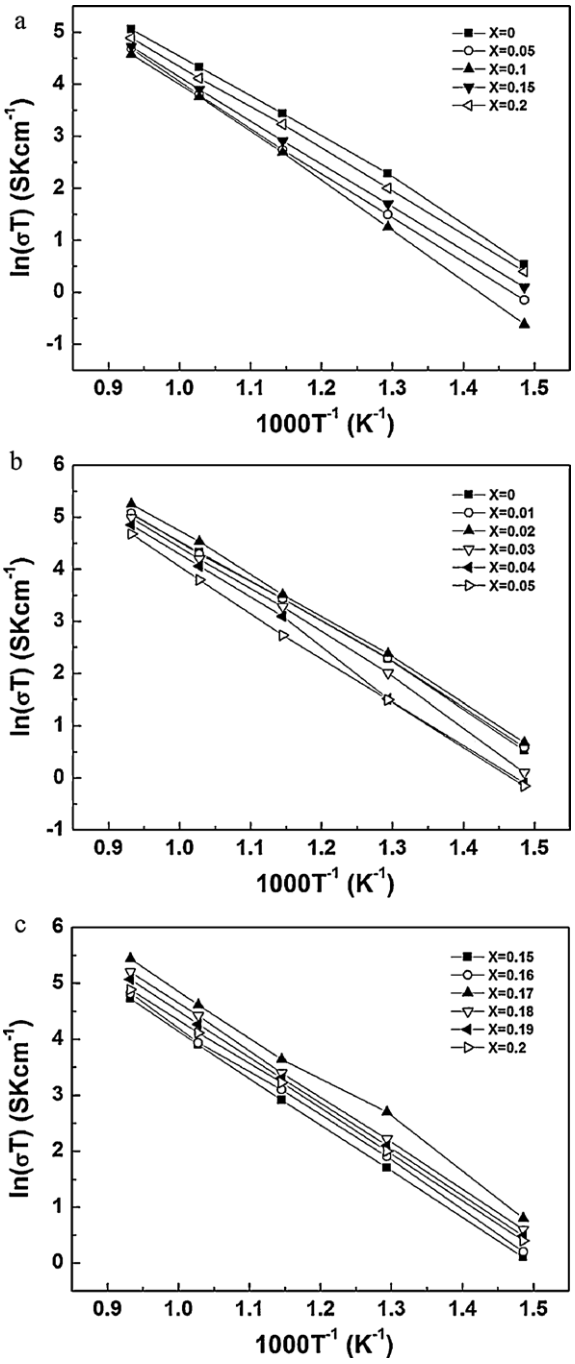

Fig. 5. Electrical conductivity of $Ce_{0.8}Gd_{0.2-x}Dy_xO_{2-\delta}$ with various Dy^{3+} contents: (a) $0 \le x \le 0.2$, (b) $0 \le x \le 0.05$, and (c) $0.15 \le x \le 0.2$.

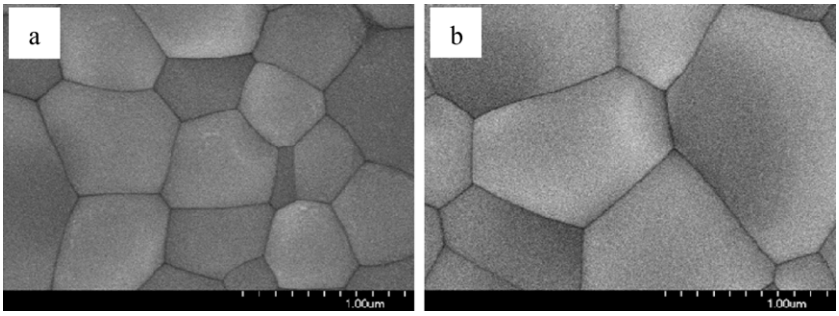

Fig. 4. FE-SEM images of sintered (a) $Ce_{0.8}Gd_{0.2}O_{2-\delta}$ and (b) $Ce_{0.8}Dy_{0.2}O_{2-\delta}$ samples.

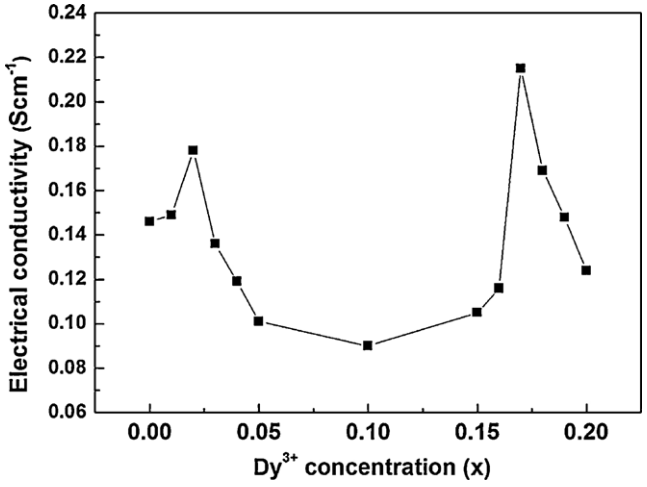

Fig. 6. Electrical conductivity of $Ce_{0.8}Gd_{0.2-x}Dy_xO_{2-\delta}$ ($0 \le x \le 0.2$) at 800 °C as a function of Dy^{3+} content.

($0.15 \le x \le 0.2$) Dy^{3+} contents, respectively. The addition of a small amount of Dy^{3+} ($0.01 \le x \le 0.02$) and of a large amount of Dy^{3+} ($0.17 \le x \le 0.19$) is found to leads to an increase in conductivity.

The electrical conductivity at 800 °C for the $Ce_{0.8}Gd_{0.2-x}Dy_xO_{2-\delta}$ ($0 \le x \le 0.2$) as a function of Dy^{3+} content is given in Fig. 6. It is clear that the electrical conductivities of the $Ce_{0.8}Gd_{0.2-x}Dy_xO_{2-\delta}$ samples with the low and high Dy^{3+} contents are much higher than those of a single doped sample, i.e., $Ce_{0.8}Gd_{0.2}O_{2-\delta}$ or $Ce_{0.8}Dy_{0.2}O_{2-\delta}$. The maximum electrical conductivity ($0.215\,S\,cm^{-1}$) is obtained with $Ce_{0.8}Gd_{0.03}Dy_{0.17}O_{2-\delta}$ at 800 °C. The conductivity ($0.078\,S\,cm^{-1}$) at 700 °C for the $Ce_{0.8}Gd_{0.2}O_{2-\delta}$ fabricated in this study is much higher than that ($0.0151\,S\,cm^{-1}$) of the $Ce_{0.8}Gd_{0.2}O_{2-\delta}$ prepared by the hydrothermal synthesis process [7]. The high conductivity of $Ce_{0.8}Gd_{0.2-x}Dy_xO_{2-\delta}$ originates from the fine grain size and high density of the $Ce_{0.8}Gd_{0.2-x}Dy_xO_{2-\delta}$ [19,20].

Mori et al. [21] have reported that the electrical conductivity increase with increase in the effective index when the oxygen vacancy level is the same. The effective index I is defined as [21]:

$$I = \left(\frac{r_c}{r_o}\right) \times \left(\frac{r_d}{r_h}\right) \quad (2)$$

where r_c, r_o, r_d and r_h are the average ionic radius of cations, the effective ionic radius of oxygen, the average ionic radius of dopants and the ionic radius of the host cation (Ce^{4+}), respectively. The effective ionic radius of oxygen r_o is expressed by

$$r_o = 1.4x\left\{\frac{(2-\delta)}{2}\right\} \quad (3)$$

where δ is the level of the oxygen vacancy. The present conductivity of the $Ce_{0.8}Gd_{0.2-x}Dy_xO_{2-\delta}$ fails to obey Eq. (2). This may be due to the fact that the value of r_o depends strongly on the composition. The high conductivity obtained here provides a significant advantage for the well-established, conventional YSZ-based electrolytes at low working temperatures.

4. Conclusions

Nano-sized $Ce_{0.8}Gd_{0.2-x}Dy_xO_{2-\delta}$ ($0 \le x \le 0.2$) powders (15–24 nm) have been successfully synthesized by the solution combustion method, using their nitrates as oxidizers and aspartic acid as fuel. The calcined $Ce_{0.8}Gd_{0.2-x}Dy_xO_{2-\delta}$ nanopowders are a ceria-based single-phase oxide with a cubic fluorite structure. $Ce_{0.8}Gd_{0.2-x}Dy_xO_{2-\delta}$ with ultra-fine grains (349–551 nm) and high density (93.3–98.7% of the theoretical density) is fabricated even at a low sintering temperature (1400 °C), using calcined nanopowders.

The electrical conductivity of the co-doped samples is strongly dependent on the content of Dy^{3+}. The conductivity of the $Ce_{0.8}Gd_{0.2-x}Dy_xO_{2-\delta}$ samples with an intermediate concentration of Dy^{3+} ($0.03 \le x \le 0.16$) is lower than that of the single-doped sample, i.e., $Ce_{0.8}Gd_{0.2}O_{2-\delta}$ or $Ce_{0.8}Dy_{0.2}O_{2-\delta}$. On the other hand, the electrical conductivity of the $Ce_{0.8}Gd_{0.2-x}Dy_xO_{2-\delta}$ samples with low ($0.01 \le x \le 0.02$) and high ($0.17 \le x \le 0.19$) Dy^{3+} contents is much higher than that of the single doped samples. The maximum electrical conductivity ($0.215\,S\,cm^{-1}$) is obtained for the $Ce_{0.8}Gd_{0.03}Dy_{0.17}O_{2-\delta}$ at 800 °C. For fabricating ceria-based electrolytes with high conductivity, it is necessary to synthesize nano-sized $Ce_{0.8}Gd_{0.2-x}Dy_xO_{2-\delta}$ powders and to control precisely the concentration of co-dopants Gd^{3+} and Dy^{3+}.

Acknowledgement

This work was supported by the Brain Korea 21 Project in 2010.

References

[1] N.P. Brandon, S. Skinner, B.C.H. Steele, Annu. Rev. Mater. Res. 33 (2003) 183.
[2] T. Mahata, G. Das, R.K. Mishra, B.P. Sharma, J. Alloys Compd. 391 (2005) 129.
[3] E. Chinarro, J.R. Jurado, M.T. Colomer, J. Eur. Ceram. Soc. 27 (2007) 3619.
[4] B. Rambabu, S. Ghosh, H. Jena, J. Mater. Sci. 41 (2006) 7530.
[5] G. Chiodelli, L. Malavasi, V. Massarotti, P. Mustarelli, E. Quartarone, Solid State Ionics 176 (2005) 1505.
[6] S. Kuharuangrong, J. Power Sources 171 (2007) 506.
[7] S. Dikmen, H. Aslanbay, E. Dikmen, O. Şahin, J. Power Sources 195 (2010) 2488.
[8] R. Raza, X. Wang, Y. Ma, B. Zhu, J. Power Sources 195 (2010) 6491.
[9] J.S. Reed, Principles of Ceramics Processing, John Wiley & Sons, Inc., New York, 1995, p.595.
[10] H. Inaba, T. Nakajima, H. Tagawa, Solid State Ionics 106 (1998) 263.
[11] W.D. Kingery, H.K. Bowen, D.R. Uhlmann, Introduction to Ceramics, John Wiley & Sons, Inc., New York, 1976, p.494.
[12] K. Egushi, T. Setoguchi, T. Inoue, H. Arai, Solid State Ionics 52 (1992) 165.
[13] [JCPDS file No. 75-0158.
[14] J. Kimpton, T.H. Randle, J. Drennan, Solid State Ionics 149 (2002) 89.
[15] B.D. Cullity, Elements of X-ray Diffraction, Addison-Wesley, Reading, MA, 1978.
[16] J.E. Blendell, C.A. Handwerker, J. Cryst. Growth 75 (1986) 138.
[17] M.P. Hamer, R.J. Brook, J. Mater. Sci. 15 (1980) 3017.
[18] J.W. Fergus, J. Power Sources 162 (2006) 30.
[19] S. Hui, J. Roller, S. Yick, X. Zhang, C. Decès-Petit, Y. Xie, R. Maric, D. Ghosh, J. Power Sources 172 (2007) 493.
[20] K. Maca, J. Cihlar, K. Castkova, O. Zmeskal, H. Hadraba, J. Eur. Ceram. Soc. 27 (2007) 4345.
[21] T. Mori, J. Drennan, J.-H. Lee, J.-G. Li, T. Ikegami, Solid State Ionics 154–155 (2002) 461.